

Investigation of Electron Contamination on Flattened and Unflattened Varian Clinac iX 6X and 15X Photon Beam Based on Monte Carlo Simulation

F. Haryanto^{1*}, M. F. Rhani², C. Anam³, S. Yani⁴

¹Department of Physics, Faculty of Mathematics and Natural Sciences, Institut Teknologi Bandung, Jl. Ganesa 10, Bandung 40116, Indonesia

²Department of Radiology, Tan Tock Seng Hospital (TTSH), 11 Jalan Tan Tock Seng 308433, Singapore

³Department of Physics, Faculty of Sciences and Mathematics, Diponegoro University, Jl. Prof. Soedarto, Semarang 50275, Indonesia

⁴Department of Physics, Faculty of Mathematics and Natural Sciences, IPB University (Bogor Agricultural University), Jl. Meranti IPB Dramaga, Bogor 16680, Indonesia

ARTICLE INFO

Article history:

Received 30 August 2021

Received in revised form 13 March 2022

Accepted 21 March 2022

Keywords:

EGSnrc code
Electron contamination
Flattening filter
Flattening filter free
Monte Carlo

ABSTRACT

The aim of this study was to characterize electron contamination of a flattened (FF) and an unflattened (FFF) Varian Clinac iX 6X and 15X photon beams using Monte Carlo (MC) simulation. EGSnrc MC technique was used to model the flattened and unflattened head and simulate dose distribution of 6X and 15X of FF and FFF photon beam in water phantom. The materials and geometrical data of FF linac were provided by Tan Tock Seng Hospital (TTSH) Singapore. The FFF linac was modeled by removing the flattening filter component in the FF linac. Phase space files were scored after flattening filter and in the phantom surface. The pshp files were analyzed to characterize the particles produced by the linac head using BEAMDP. The contaminants contribute around 1 % and 2 % in the pshp1 for flattened and unflattened beams, respectively. The photons are scattered in small-angle in the range of 0 – 4°. The contaminant electron contributes up to one hundredth compared to the photons. The increase of field area affects the increase in contaminants and penumbra width due to the increasing number of particle scattered out of the field area. The unflattened beam affects the increase in the number of electron contamination and surface dose. The penumbra width of the flattened beams was smaller than the unflattened beams for the same field size and energy.

© 2022 Atom Indonesia. All rights reserved

INTRODUCTION

At present, MC technique is a widely used tool in radiation therapy for calculating dose distribution and modeling head linac in radiotherapy by simulating the trajectories of the particles through the desired region. This method can produce highly accurate and reliable results but requires a long simulation time. Some MC codes used in radiotherapy such as EGSnrc/BEAMnrc-DOSXYZnrc [1,2], MCNP [3], Geant4 [4,5], Fluka [6], and PENELOPE [7,8] have been conducted to

characterize linac output spectra and dose distributions inhomogeneity and inhomogeneity phantom. The simulation outputs acquired by several investigators using the same code differ from each other due to the distinction in the system platforms and cross-section data provided by MC packages. Accurate dose distribution with the MC codes requires careful identification of head geometry, the incident electron energy, and full width at half maximum of the beam [9]. The linac head components such as target, primary collimator, vacuum window, flattening filter, ionization chamber, JAWS X, and Y and multileaf collimator (MLC) function in generating the desired photon or electrons during treatment.

*Corresponding author.

E-mail address: freddy@fi.itb.ac.id

DOI: <https://doi.org/10.17146/aij.2022.1180>

Linac head flattening filter (FF) serves to produce a homogeneous beam profile generated by the bremsstrahlung phenomenon at a certain depth, usually placed in the central beam axis with a conical shape depending on the energy of the linac. FF is made from materials with high atomic numbers, such as copper (Cu). New treatment technologies that are widely developed today require high-energy photon beams, so it does not require homogeneous beams such as intensity-modulated radiation therapy (IMRT), stereotactic body radiation therapy (SBRT) and linac-based radiosurgery. In these treatment techniques, FF is not required. Several studies related to flattening filter free (FFF) have been conducted at different energies [10,11]. They reported that removing the FF increased the dose rate and reduce the head scatter [12-14], electrons and neutrons contamination [15,16], out-of-field and penumbra doses [11,17,18]. The increase in particle contaminants in the FFF beam is caused by the bremsstrahlung photon from the X-ray target interacting with the electrons and nucleus of Cu and producing particle contamination (electron and neutron) after the FF [15,16]. This means that a higher dose will accumulate on the surface of the patient or phantom. It was found that contaminating electrons shift the depth of maximum dose toward a shallower depths with field size in high energy photon beams [19]. Several investigators reported that the FF and the ionization chamber are the main sources of particle contamination because these components are located in the central beam axis [20,21].

In this study, electron contamination was investigated in the flattened (FF) and unflattened (FFF) Varian Clinac iX 6X and 15X photon beams using the EGSnrc MC technique. Therefore, the dose calculation on the clinical treatment planning system can consider the effect of electron contamination from both Linacs.

MATERIAL AND METHODS

A Varian Clinac iX medical accelerator of 6 and 15 MV FF and FFF photon beam was modeled using EGSnrc-based BEAMnrc Monte Carlo code. The linac head material and geometry had been provided by the manufacturer (Varian Medical Systems, Palo Alto, CA, USA). The measurement data were obtained at SAD 100 cm in a $40 \times 40 \times 40$ cm³ water phantom.

Monte carlo simulation

An EGSnrc-BEAMnrc platform [22] was used to design a Varian Clinac iX 6 MV and 15 MV photon beam. The measurement data of FF linac head, e.g., profile dose and percent depth dose data were provided by Tan Tock Seng Hospital (TTSH) Singapore. The linac head with FF components in this work (target, primary collimator, vacuum windows, flattening filter, ion chamber, JAWS X, and Y and multileaf collimator) is shown in Fig. 1. The FF is set to vacuum material to model Linac FFF. The linac manufacturer has provided complex machine drawing and material tables which are very useful in modeling these linacs. Nevertheless, some important parameters such as incident electron energy, beam geometry, and radial intensity (full width at half maximum/FWHM) were obtained using the trial and error method by comparing simulated and measured percentage depth doses and lateral beam profiles in a water phantom.

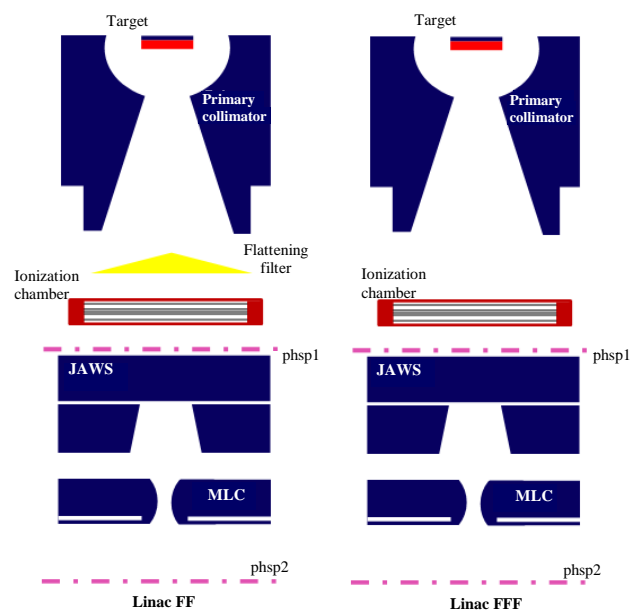


Fig. 1. Sketch of Varian Clinac iX 6 MV photon beam treatment head components.

The treatment head was divided into two parts; First part: patient-independent components (target, primary collimator, vacuum window, flattening filter, and ionization chamber) and the second part: the patient-dependent components (Jaws Y and X and MLC).

The first step of the simulation was started by generating phase-space (phsp) files below the ionization chamber or above the patient-dependent part using ISOURC = 19. The obtained phsp files were used in the second part of the patient-dependent components of the treatment head. This

step was done for 6 and 15 MV FF and FFF photon beams. Linac 6 and 15 MV have a different target and FF geometry but have the same material compositions. The second step of head simulation, the phsp files were generated below the ionization chamber as particle sources for the second part of linac. The ISOURC = 2 was chosen as source and the phsp placed above the JAWS Y to create phsp files above the water phantom surface at distance of 80 cm from target. This source makes it possible to use the generated phsp files in any scoring plane to be used as a particle resource in other simulations. The particles in the phsp file can pound any CM of the specified component.

In this work, 1×10^9 incident electrons were simulated for flattened and unflattened 6 MV and 15 MV beams. The phsp files were saved for each simulation. The phsp data from patient-independent components (below the ionization chamber) of 6 or 15 MV beams can be used multiple times for varied patient-dependent parts of the treatment head (different set of X and Y-jaws or MLC). The energy of simulated linac was varied from 6,0 to 6,4 MeV with radial intensity modeled as a Gaussian distributions.

BEAMnrc and DOSXYZnrc simulation parameters were set as default settings (no variance reduction technique applied). The electron range rejection was set to 1 MeV (ESAVE). The simulation used 4×10^8 histories for patient-dependent components. All calculations were performed by core i3 CPU (8 cores) composed of eight 3.2 GHz under Linux Ubuntu. The beam characteristics such as percent depth doses (PDDs) and lateral beam profiles were analyzed using statdose. The BEAMDP code was used to analyzed mean energy, spectral distribution, angular distribution, and X-Y scatters of phsp files [23]. The analysis program reads an input file, which includes the particle type (all particles, photon, electron, or positron), the phsp file name, the orientation of the region, dimensions of the scoring regions, and the number of bins in every region. In the case of plotting the spectral distribution, the maximum and minimum energy of the particles to be processed need to be specified. For angular distributions, the user needs to input the maximum and minimum angle. As for the mean energy and fluence, the shape of bin areas can be either square or annular. The number of bin area and the maximum radius of the region of interest need to be specified for all distributions calculated.

Dose calculations

The dose distributions of a $40 \times 40 \times 40 \text{ cm}^3$ virtual water phantom positioned at 80 cm from the target have been computed. This type of phantom is recommended by Varian Medical Systems, Palo Alto, CA, USA. The dosimetric characteristics of flattened and unflattened 6 MV and 15 MV photon beams such as PDDs and lateral dose profiles were calculated in small volumes called voxels; each voxel has a different dimensions depending on beam energy and field size to reduce simulation time and obtain better results [2]. Dose distributions for several field sizes of 6×6 , 10×10 and $20 \times 20 \text{ cm}^2$ have been computed.

The PDDs curves for FF and FFF beams were calculated in the central beam axis of the water phantom. Lateral beam profiles for 6X and 15X flatten and unflatten beams were studied. To characterize this feature, the penumbra width (distance between off-axis doses of 80 % and 20 % (P_{80-20} %)) and location of field edge at the off-axis dose of 50 % (FWHM) were analyzed for each field size (Fig. 2). These calculated beam profiles were normalized to the maximum dose at the central axis and evaluated at a depth of 10 cm.

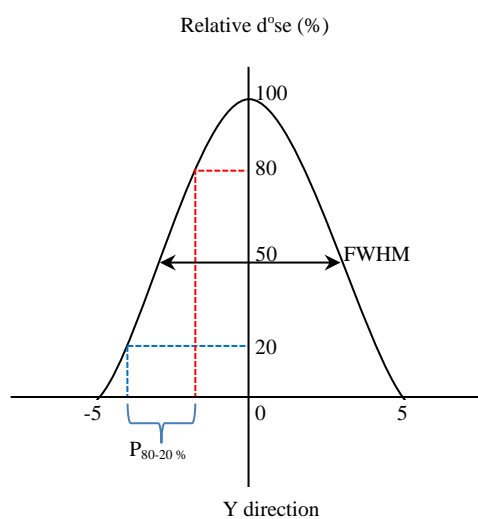


Fig. 2. Characterization of lateral beam profiles.

Surface dose, local dose difference, and lateral dose profile characteristics

Surface dose or skin dose flattened and unflattened 6 MV and 15 MV beams is the dose calculated at the phantom surface (0 – 5 cm). The dose was calculated for 6×6 , 10×10 , and $20 \times 20 \text{ cm}^2$ open field sizes for all particles, photons, and electrons. The build-up effect in the surface region can cause the skin-sparing effect or the dose accumulates on the surface of the target or patient [12].

The following formula calculated local dose differences between two points for flattened and unflattened beam using Eq. (1):

$$Local\ dose\ difference = \frac{|Dose_{FF} - Dose_{FFF}|}{Dose_{FF}} \quad (1)$$

Electron contamination

To calculate the electron contamination from phsp files, every particle position, direction, and energy need to determine at the scoring plane after flattening filter and phantom surface. The photon and electron extracted from phsp file were scored in the phantom surface for 6×6, 10×10, and 20×20 cm². Phsp files containing photon and electron were used to simulate in DOSXYZnrc to get a relative absorbed dose of photons and contaminating electrons, respectively.

RESULTS AND DISCUSSION

The statistical uncertainties obtained for all simulations were less than 0.1 % for at all measurement voxels inside the field for PDDs and lateral beam profiles. Meanwhile, this value was less than 1.1 % in the out-of-field and the penumbra regions.

Particles characterization on phsp1

For every particle that passes through the scoring plane, an entry in the phsp files was created including charge, energy, x and y position, the direction cosines for the x- and y-axis, the direction cosine of the angle for the z-axis and position of the particle energy, the particle weight, other particle history information named LATCH.

Table 1. Information of particles on phsp1.

Linac energy	Incident particles from original source	All particles	Photon	Electron	CPU time (hours)
6X FF	34172727296	86978245	86730104	248141	6.53
6X FFF	12137300992	89875282	88847303	1027979	3.65
15X FF	5019129344	86548522	86177448	371074	2.73
15X FFF	2404502272	87319929	86863646	456283	2.15

Table 1 shows a resume of the number of particles in the phsp files scored below the ionization chamber and the CPU time used for the BEAMnrc simulations of the 6 and 15 MV FF and FFF Linac using an electron beam of 6.4 and 15.4 MeV on the bremsstrahlung target. The phsp files have the same file capacity of 2.4 GB. Initial incident electron energy, linac’s geometry, and the number of histories affect the simulation time (CPU time). High energy electron hitting the target will produce more photon bremsstrahlung than low

energy linac, so the simulation time will be shorter. The omission of the FF caused a substantial increase of electron contaminants for 6 MV and 15 MV beams. The amount of 1.2 % particles in the unflattened 6 MV phsp file is electrons.

The phase-space files were characterized using the BEAMnrc data processor, BEAMDP. Particles fluence, energy fluence, mean energy profiles, spectral, and angular distributions above JAWS Y were investigated. These parameters cannot be measured experimentally.

Bremsstrahlung photons released from the tungsten target and the primary collimator are highly forward peaked. The 6 MV and 15 MV beam contain high intensity photons with the highest energy at the beam axis and lowest in the out-of field. The composition and the material of the target affect the bremsstrahlung photons released from the beam.

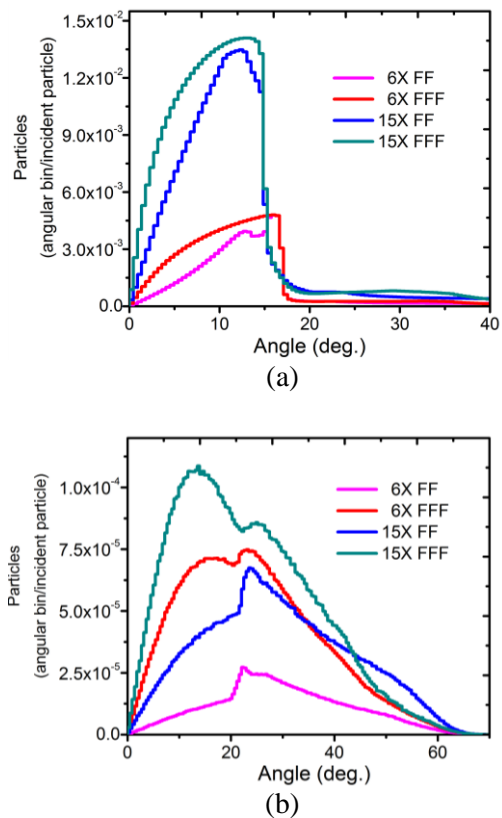


Fig. 3. Angular distribution of (a) all particles and (b) electron calculated below flattening filter (phsp1) for 6X and 15X FF and FFF photon beams.

Angular distributions of all particles and electrons produced by linac head were recorded over the scoring plane below the FF position (20 cm from target) as a function of the scattered angle of photons and electrons. The particles are scattered at angles of less than 20° from the beam axis (Fig. 3(a)). As the particles are collimated only by a primary collimator, the particles scattered from the target with a large angle are present in the scoring plane for flattened and unflattened linac. In contrast, the

opposite phenomenon occurs with electrons contamination. These particles scatter at a larger angle, which indicates that most of the contamination was produced due to interaction between photons created from the target and the linac component that it passed (Fig. 3(b)). The contaminants are dispersed at large angles in the range 0 to 60° from the central beam axis. These contaminants contribute low scattered particles equal to one hundredth of the number of photons in the scoring plane for unflatten and flatten 6X and 15X photon beams.

The mean energy of the 6 and 15 MV photon beams were investigated by simulating contaminants from an angle of 0 to 90°, and the results are shown in Fig. 4(a). In this step, the X_{min} , X_{max} , Y_{min} , Y_{max} , and the number of bins were set to -20 cm, 20 cm, -20 cm, 20 cm, and 200 bins, respectively. The mean energy curves of all particles in phsp files for flattened and unflattened 6 and 15 MV photon beam in the Y direction between $Y=-10$ cm and $Y=10$ cm is relatively low due to the flattening filter, but not for the unflattened beam. The mean energy outside $Y=-10$ cm and $Y=10$ cm is low. The particles mean energy peaks of 6X FF, 6X FFF, 15X FF and 15X FFF were respectively 1.25 MeV, 1.34 MeV, 2.5 MeV, and 2.75 MeV. The distribution of mean energy of the contaminant is smaller at the beam axis compared to the photons graph inside the field as shown in Fig. 4(b). The mean energy of electron is relatively flat in the range of -10 to 10 cm field for a 6X unflattened beam.

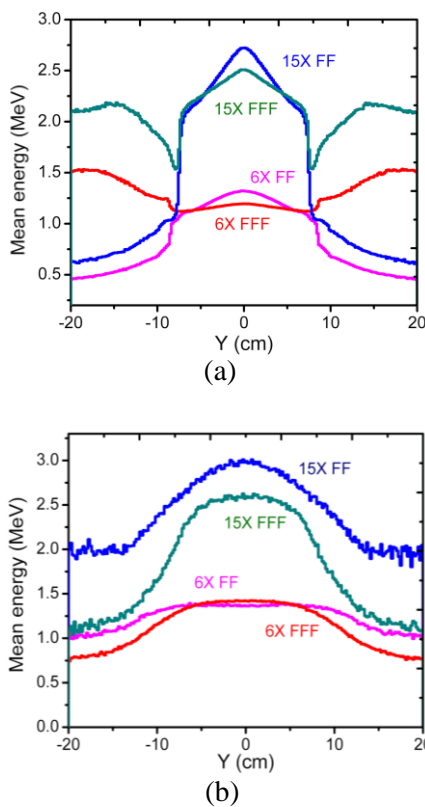


Fig. 4. Mean energies of (a) all particles and (b) electron calculated below flattening filter (phsp1) for 6X and 15X FF and FFF photon beams.

Figure 5(a) shows the fluence profile of photons and electrons in phsp files as a function of the distance to the central beam. The photons are scattered at large angles as a result of interaction with the linac components such as the primary collimator, FF, and vacuum window. The presence of a flattening filter was clearly visible in this graph. The graph shows bell-shaped curves because the shape of the curve resemble a bell. The FWHM of all particles planar fluence for 6XFF, 6XFFF, 15XFF, and 15XFFF was 15.2 cm, 12 cm, 12 cm, and 9.2 cm. These values was relatively high due to the existence of a flattening filter. Flattening filter was used to homogenize the beam and increase the average value of photon energy by eliminating the low energy photons. The fluence curve of the unflattened beam has a sharper peak than the flatter one. Meanwhile, electrons were distributed normally along the Y direction in the range of -20 to 20 cm (Fig. 5(b)). The fluence decreases gradually from the central beam axis, most of the electrons concentrated in the center of the beam in phsp files for flattened and unflattened beams. The FWHM of electron planar fluence for 6XFF, 6XFFF, 15XFF, and 15XFFF are 24 cm, 14.6 cm, 17.4 cm and 14 cm, respectively.

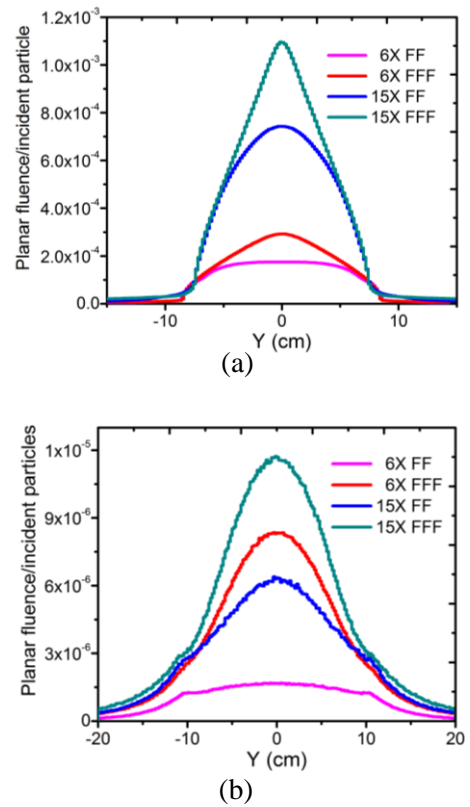


Fig. 5. Planar fluence of (a) all particles and (b) electron calculated below flattening filter (phsp1) for 6X and 15X FF and FFF photon beams.

The spectral distributions of the flattened and unflattened beam have the same trend (Fig. 6(a)). This figure shows the energy spectral of particles in phsp files as a function of length from the central beam. The intensity of unflattened photon beam is larger than the flattened linac for 6X and 15X Linac. The FF hardens the beam more at the center of the beam than at the peripheral regions but not for the FFF beam. In Fig. 6(b), the photon and electron energy spectra are presented for the 6 MV beams with a field size of $10 \times 10 \text{ cm}^2$ at the phantom surface. For photons, the energy spectra show a much defined peak at around 0.5 MeV and there is a spike in, while the spectrum of contaminant electrons peaks at slightly lower energy, around 0.3 MeV. It is also clear from these spectra that photons' fluence at the peak is four orders of magnitude higher than those of contaminant electrons.

X-Y scatter plot from phsp files in BEAMDP describe a plot of the X-Y positions of particles (photon, electron, positron, and all particles) for the specific number of particles and area. Figure 7 shows the scatter plot 6X and 15X flattened and unflattened beam for 1000 electrons inside the $30 \times 30 \text{ cm}^2$ area. The electron contamination scattered to the large X and Y directions.

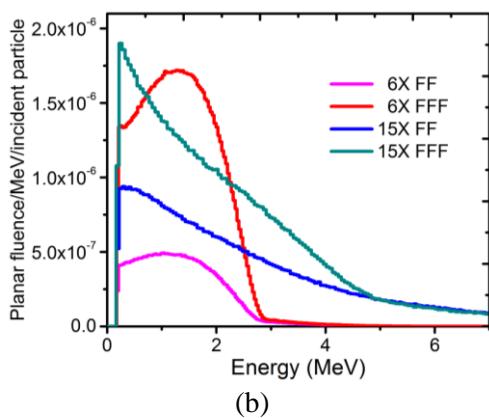
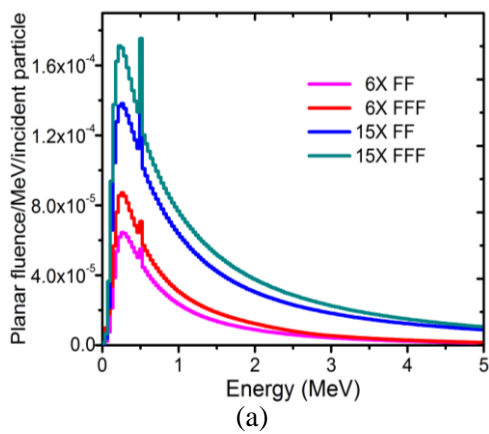


Fig. 6. Spectral distribution of (a) all particles and (b) electron calculated below flattening filter (phsp1) for 6X and 15X FF and FFF photon beams.

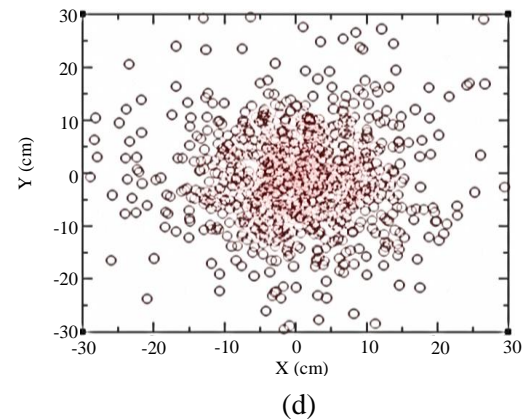
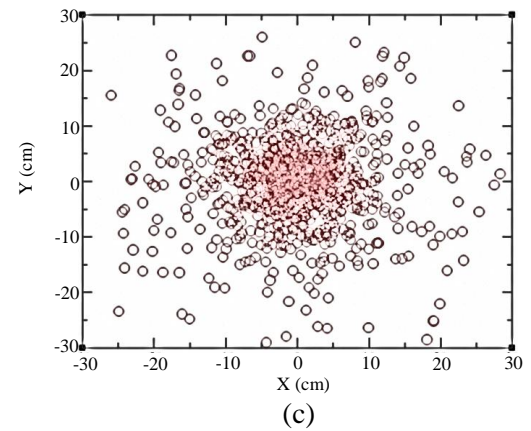
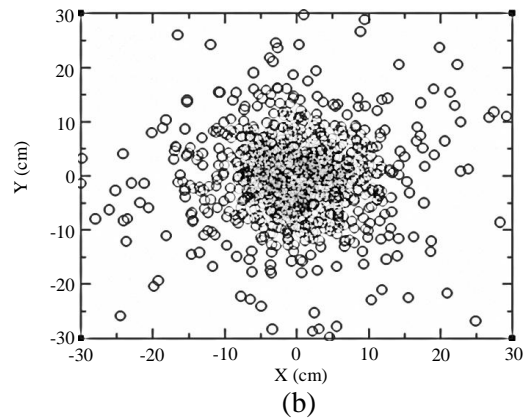
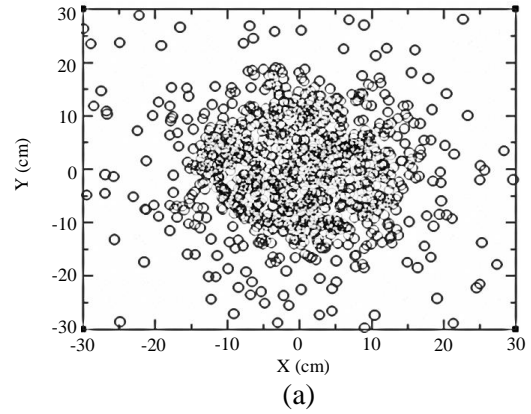


Fig. 7. Scatter plot of 1000 contaminants electron calculated below flattening filter for (a) 6X FF, (b) 6X FFF, (c) 15X FF, and (d) 15X FFF photon beams.

Particles characteristics on phantom surface (phsp2)

The second phsp files scored 80 cm from the target for open fields 6×6, 10×10, and 20×20 cm². The phsp file capacity was 2.4 GB. Table 2 describes the information of particles in the scoring region.

Table 2. Information of particles on phsp2.

Field size	Linac energy	Incident particles from original source	All particles	Photon	Electron
6×6	6X FF	97297350656	84538226	84412212	126014
	6X FFF	31210203136	86129708	85520908	608800
	15X FF	12619525120	78067556	77846739	220817
	15X FFF	5896756224	86533708	86235816	297892
10×10	6X FF	34172727296	86978245	86730104	248141
	6X FFF	12137300992	89875282	88847303	1027979
	15X FF	5019129344	86548522	86177448	371074
	15X FFF	2404502272	87319929	86863646	456283
20×20	6X FF	8068560384	88111332	87709728	401604
	6X FFF	3225054208	83240743	81804465	1436278
	15X FF	1347994752	88004566	87525595	478971
	15X FFF	807225792	89208217	88529236	678981

All the angular distribution, mean energy, planar fluence, and spectral distribution for all particles and electrons were generated using the phsp files scored at phantom surface using BEAMDP with the same parameters used for the 10×10 cm² field (Figs. 8 and 9).

Angular distribution of all particles for 6XFF, 6XFFF, 15XFF, and 15XFFF 10×10 cm² field is presented in Fig. 7(a). The photons are scattered in small-angle in the range of 0 – 4° and peak photon energy fluence in 2.5°. The scattered angles of maximum photon fluence increase with the increase of field size in flattened and unflattened beams. This angle was smaller than particles below FF because MLC collimated the beam before entering the phantom surface. Meanwhile, electrons have a wider scattering angle (0 – 20°) and peak electrons energy fluence in 6.3°, 5.0°, 4.5°, and 3.6° for 6XFF, 6XFFF, 15XFF, and 15XFFF, respectively. The electron contaminant contribution was only one hundredth of the total number of particles in the phsp file. Beam energy affects the electron scattering angle (the electrons will have a large scattering angle if the electron energy is low). Electron's mean energy was decreased gradually with the space from the central beam axis and had the maximum value at the center of the 10×10 cm² field as shown in Fig. 8(b). Mean energy value for 6X FF, 6X FFF, 15X FF, and 15X FFF was 1.75 MeV, 1.5 MeV, 4.5 MeV, and 3.7 MeV, respectively. The mean energy decreases for 6 and 15 X unflatten beams. Mean energy of photons 6X and 15X flatten the beam was decreased inside the field of 6×6, 10×10, and 20×20 cm².

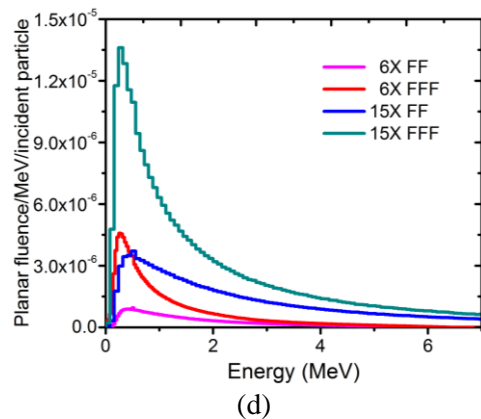
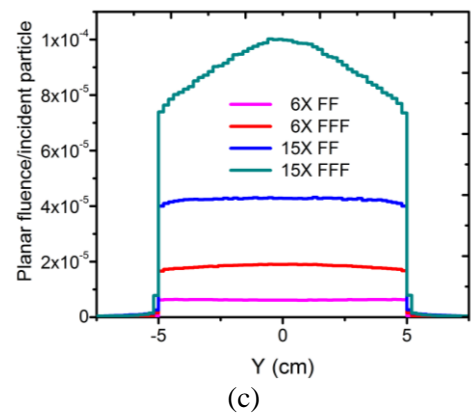
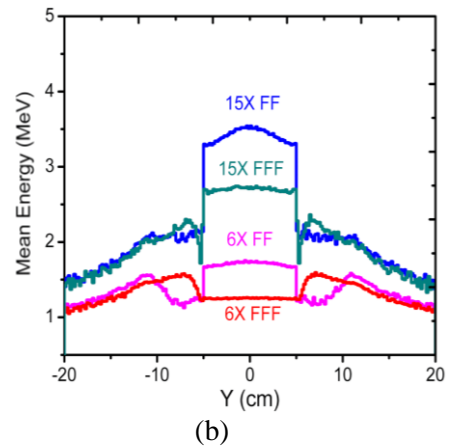
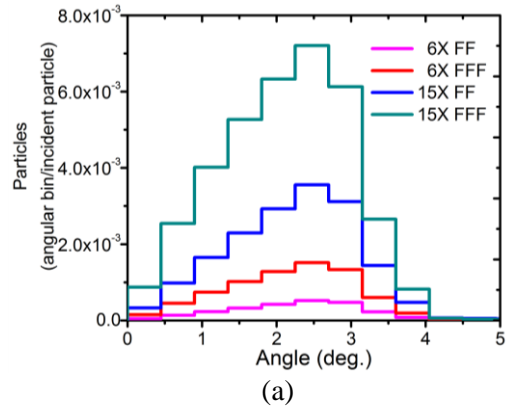


Fig. 8. Angular distribution, mean energy, planar fluence and spectral distribution of all particles along Y direction in phsp2 for 6X and 15X FF and FFF photon beams.

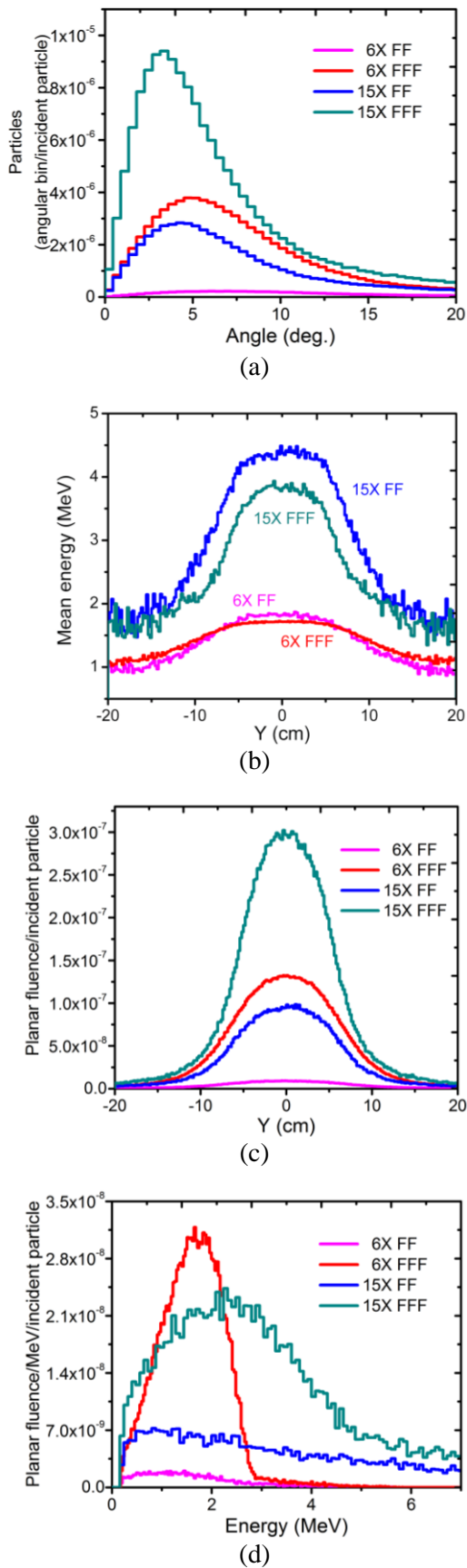


Fig. 9. Angular distribution, mean energy, fluence, and spectral distribution of electron in phsp2 field size $10 \times 10 \text{ cm}^2$ for 6X and 15X FF and FFF photon beams.

Figures 8(c) and 9(c) show the values of the fluence calculated for $10 \times 10 \text{ cm}^2$ in a square bin of 0.5 cm and 15 cm half-width. Comparing these figures, electron contamination is responsible for the shape of the figures scattered over large scattering angles. This scattering angle increases with the increasing of field width due to the electron contamination with a large scattering angle from phsp1 reduced by JAWS X and Y and MLC. The total planar fluence for all particles which photons give the main contribution is relatively constant inside the field and decreases dramatically out of the field ($x < -5 \text{ cm}$ and $x > 5 \text{ cm}$). The horn geometry was not invisible in planar fluence for flattened beams (6X and 15X). The FWHM of electron planar fluences for 6 MV FF, 6 MV FFF, 15 MV FF, and 15 MV FFF were 15.8, 14, 13.4, and 11.6/ MeV/incident particles, respectively. Figures 8(d) and 9(d) present particle's energy spectra for field size of $10 \times 10 \text{ cm}^2$ 6X and 15X flattened and unflattened beams in the phantom surface. For photons, the spectral distribution has a very sharp peaks at 0.5 MeV. Meanwhile, the spectra of electron contaminations have peaks at a higher energy than photons, around 1.47 MeV, 1.68 MeV, 0.88 MeV, and 2.24 MeV for 6X FF, 6X FFF, 15X FF, and 15X FFF, respectively. From this spectrum graph it can be seen that there are 10^3 times more number of photons than electron contaminations in the scoring plane.

PDDs and lateral dose profiles

The phantom dose calculation was performed using the EGSnrc-DOSXYZnrc user code. The treatment fields were simulated using the phsp files generated in the treatment linac head simulation for flattened and unflattened 6X and 15X beams. For phantom dose calculation (depth doses and lateral dose profiles), 3×10^8 particles were used. PDDs and lateral dose profiles calculated using Monte Carlo simulations were illustrated in Fig. 10. To investigate the effect of the repeated use of particles on the statistical uncertainty as had been investigated by many previous investigators, a number of simulations with DOSXYZnrc calculations were carried out in a homogeneous water phantom by recycling the photon and electron in a scoring plane. The results obtained indicate that the repeated use of particles greatly affects the uncertainty value and changes the behavior. In this study, it was found that the increase in the relative uncertainty value was greatly influenced by depth.

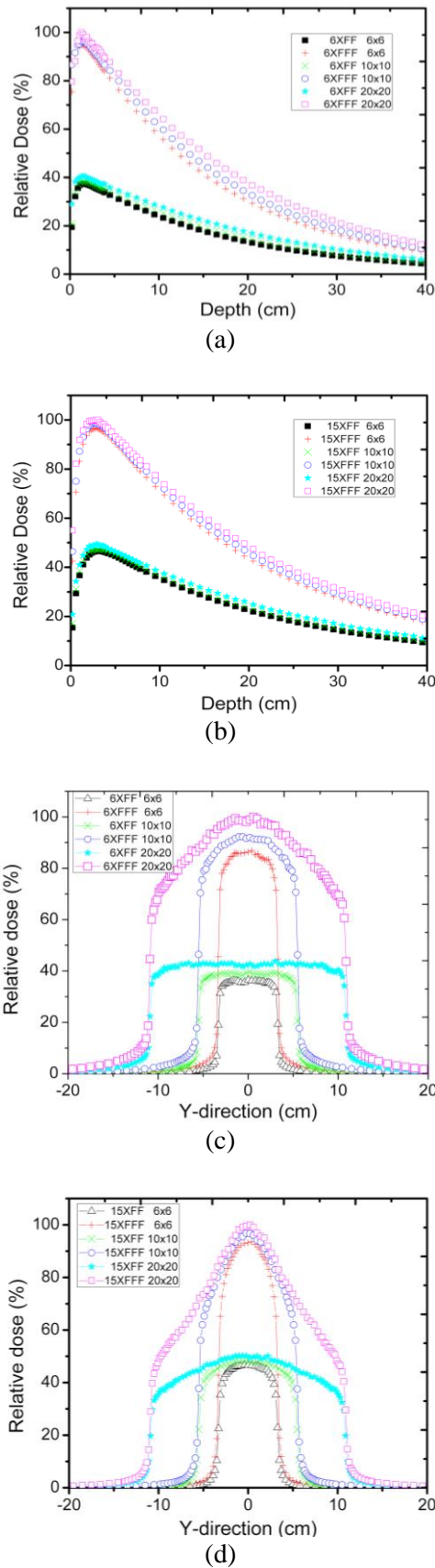


Fig. 10. Depth-dose and beam profiles curves for the 6×6, 10×10, and 20×20 cm² field, with the 6X and 15X FF and FFF beam (SSD = 100 cm). Curves were normalized to maximum dose for every energy beam. The beam profiles scored at 10 cm depth from the phantom surface.

PDDs 6X and 15X FF and FFF beam field size 6×6, 10×10 and 20×20 cm²

Figures 10(a) and 10(b), DOSXYZnrcMonte Carlo simulation results are shown depth dose curves of flatten and unflatten beams. This figure shows the depth dose curves in 40×40×40 water phantom. Doses were normalized at maximum dose for all the curves. The maximum dose in Figs. 10(a) and 10(b) were obtained from 6XFFF and 15XFFF beams, respectively. The underlined result in this study is that the d_{max} at 6X FF changes with changes in field size, d_{max} for field size 6×6 cm² was 1.5 cm, whereas for the most significant field 10×10 and 20×20 cm² the depth declined to 1.3 cm. The change in d_{max} was created by an increase in the number of scattered particles over a large field size.

Meanwhile, the d_{max} of unflattened beams was shifted to shallow depth due to the enhancement in the contribution of the electron contaminant at larger field sizes. The contaminant electron was increased with the rise of field sizes for flattened and unflattened beams (Table 2). It is also usually found a slight shift of the d_{max} to shallower depths when the field size is enhanced for 6X and 15X photon beams. The d_{max} of 15X unflatten beam was shifting to the larger depth (6×6 cm², d_{max} =3.1 cm; 10×10 cm², d_{max} =3.3 cm; and 20×20 cm², d_{max} =3.5 cm) whereas d_{max} of the flattened beam has same depth at 2.9 cm (this value changed to shallow depth compared with the unflattened beam).

Table 3. Local differences of all particles and contaminant electrons flatten and unflatten beam 6X and 15X photon beam.

Depth (cm)	Local differences											
	All particles						Contaminant electron					
	6X		15X		20x20		6X		15X		20x20	
0.60	1.83	1.72	1.3	1.41	1.41	1.41	2.01	2.22	2.74	1.29	1.29	1.23
1.00	1.60	1.52	1.46	1.26	1.27	1.24	1.63	1.65	1.60	1.18	1.17	1.16
1.40	1.53	1.49	1.46	1.19	1.18	1.13	1.54	1.52	1.45	1.12	1.13	1.11
2.10	1.51	1.48	1.43	1.1	1.10	1.05	1.50	1.48	1.40	1.09	1.09	1.08
3.10	1.5	1.47	1.46	1.06	1.07	1.03	1.49	1.47	1.38	1.06	1.06	1.03
4.20	1.48	1.45	1.42	1.05	1.03	1.03	1.49	1.47	1.44	1.03	1.04	1.02
5.00	1.47	1.45	1.42	1.03	1.03	1.01	1.46	1.46	1.42	1.03	1.02	0.98
10.50	1.39	1.36	1.32	1.00	1.00	0.97	1.39	1.38	1.33	0.99	0.99	0.95
20.50	1.26	1.23	1.19	0.94	0.92	0.91	1.27	1.22	1.17	0.99	0.92	0.89

Table 3 shows the local dose difference of flattened and unflattened beam 6X and 15X for various square field sizes calculated using equation (1). Unflattened beam affects depth dose value at each depth, not only on the phantom surface. The same results can also be seen in Figs. 10(a) and 10(b). The local difference values reach a factor of

2 on the phantom surface, especially in 6XFFF with large field size, and continue to shrink gradually as the depth increases. This is due to the higher amount of electron contaminants produced from this beam.

Lateral dose profiles 6X and 15X FF and FFF beam field size 6x6, 10x10 and 20x20 cm²

Figures 10(c) and 10(d) show the dose distribution of DOSXYZnrc Monte Carlo simulation results calculated along the Y direction. The voxel dimension was different from the PDDs one. On the other hand, the voxel arrangements for different field sizes were different from each other to reduce the simulation time and obtain the best dose distribution results. Figure 10(c) shows lateral dose profiles curves for 6XFF and FFF beams in various field sizes and Fig. 10(d) shows for 6XFF and FFF beams in various field sizes. The lateral beam profiles scored 10 cm depth from the phantom surface for all field sizes and normalized at maximum dose for all the curves in each figure.

Table 4. Lateral beam profiles characteristics of all particles and contaminant electrons flattened and unflattened beam 6X and 15X photon beam.

Field size (cm ²)	6X				15X			
	Penumbra width (P ₈₀₋₂₀ %) (cm)		FWHM (X ₅₀ %) (cm)		Penumbra width (P ₈₀₋₂₀ %) (cm)		FWHM (X ₅₀ %) (cm)	
	FF	FFF	FF	FFF	FF	FFF	FF	FFF
6x6	0.36	0.49	6.63	6.62	0.60	0.69	6.56	6.53
10x10	0.38	0.42	11.03	11.00	0.77	2.06	10.93	10.77
20x20	0.52	3.77	21.82	21.65	2.85	7.22	21.58	19.48

Table 4 shows the calculations obtained from the penumbra width and field edge at several field sizes at 10 cm depth after normalization. Figures 9(c) and 9(d) show the lateral dose profile curves of the 6X FFF beams and it was observed to be sharper than that of the 6XFF for every field size at 10 cm depth. It means that the penumbral width of 6XFF was larger than 6XFFF for all fields. The increase of fields affects the rise of penumbra due to the increasing of scattered particles in the out of field area. The same characteristic of the penumbra was also spotted for 15X FF and 15X beam. The percentage variation of the penumbra with increasing field size was higher for the high-energy than for the low-energy beams. The sharper lateral beam profile for unflattened beams at different field sizes was caused by FWHM. The field edge of unflattened beams was tighter than flattened beams both for 6X and 15X. The surface

dose and build-up region at 0 – 5 cm from the phantom surface of 15XFF and FFF photon beams were evaluated only for 6x6 and 20x20 cm² field sizes for all particles as shown in Figs. 11(a) and 11(b). The simulation results of the contaminant electron effect in the build-up region are summarized in Table 5. The local dose difference table shows that the surface dose increased linearly with field size for all beams. At the FFF beam, the large number of electron contaminants and low-energy photons arriving at the phantom surface causes an increase in the surface dose.

Table 5. Local differences of contaminant electrons flattened and unflattened beam 15X photon beam for field sizes 6x6 and 20x20 cm².

Depth (cm)	Local differences					
	6X			15X		
	6x6	10x10	20x20	6x6	10x10	20x20
0.60	1.83	1.72	1.3	1.41	1.41	1.41
1.00	1.60	1.52	1.46	1.26	1.27	1.24
1.40	1.53	1.49	1.46	1.19	1.18	1.13
2.10	1.51	1.48	1.43	1.1	1.10	1.05
3.10	1.5	1.47	1.46	1.06	1.07	1.03
4.20	1.48	1.45	1.42	1.05	1.03	1.03
5.00	1.47	1.45	1.42	1.03	1.03	1.01

The statistical uncertainty of the simulation results is significant with increasing depth, especially for the electron contamination curve. The lateral dose profiles along the Y direction of MC calculation for all particles, photons, and electrons are presented in Figs. 11(c) and 11(d). The shapes of the measured profile along the Y-axis show that the profile presents asymmetric behavior along the entire field. The statistical uncertainties were less than 5 % for all particles and photon profile dose curves inside the field and less than 10 % outside the fields due to the smaller number of particles outside the field than inside. Meanwhile, the small amount of contaminant affects the higher statistical uncertainty of the dose profile curve inside and outside the fields. The results for unflattened 6X photon beam with various field sizes are in line with our previous study on electron contamination for small field dosimetry [1,20]. A large field size will result in more contamination particles and a larger surface doses. In addition, Wang et al. (2012) and Mohammed et al. (2017) showed that surface dose increase linearly with the increasing of open field size for both flattened and unflattened beams [12,24].

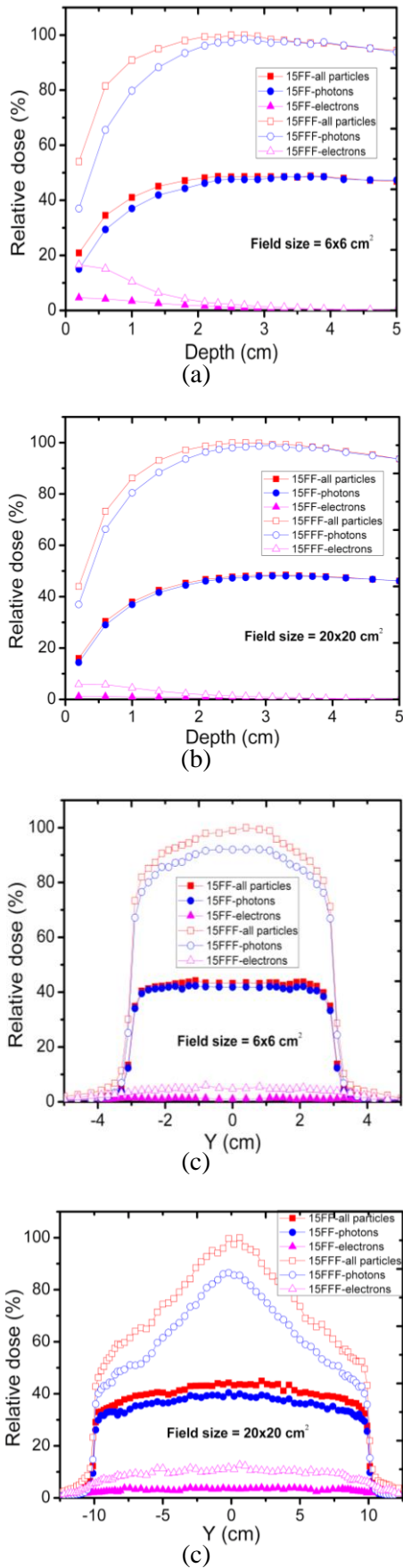


Fig. 11. Depth-dose and beam profiles curves for the 6x6, and 20x20 cm² field of electrons and photons are defined as the dose calculated at 1 – 5 cm from water phantom surface for 15X FF and FFF photon beams.

CONCLUSION

In this current work, the head of Varian Clinac iX 6 and 15 MV FF and FFF photon beams for fields 6x6, 10x10 and 20x20 cm² has been modeled. The electron contamination was scattered in a larger angle than a photon in the phantom surface. The unflattened beam affects the increasing number of electron contamination and low-energy photons and causes an enhancement in the surface dose. For the same field size and energy, the penumbra width of flattened beams was smaller than the unflattened beams. The unflattened beam affects the increasing the number of electron contamination and surface dose. For the same field size and energy, the penumbra width of flattened beams was smaller than the unflattened beams.

ACKNOWLEDGMENT

This study was supported by Program Penelitian Kolaborasi Indonesia, World Class University Program Indonesia (No. 441/UN7.P/HK/2020). The authors thank the National University Cancer Institute Singapore for Linac's geometry and material data.

AUTHOR CONTRIBUTION

Freddy Haryanto contributed in data analysis and as primary writer in this manuscript. Mohamad Fahdillah Rhani was responsible for collecting data of material and geometry of Linac. Choirul Anam and Sitti Yani contributed by running the Linac 6X and 15X simulation, respectively.

REFERENCES

1. S. Yani, M. F. Rhani, R. C. X. Soh *et al.*, *Int. J. Radiat. Res.* **15** (2017) 275.
2. I. G. E. Dirgayussa, S. Yani, M. F. Rhani *et al.*, *AIP Conf. Proc.* **1677** (2015) 040006.
3. N. Shagholi, H. Nedaie, M. Sadeghi *et al.*, *J. Adv. Phys.* **6** (2014) 1006.
4. M. Fiak, A. Fathi, J. Inchaouh *et al.*, *Moscow Univ. Phys. Bull.* **76** (2021) 15.
5. M. Assalmi, E. Y. Diaf and N. Mansour, *Rep. Pract. Oncol. Radiother.* **25** (2020) 1001.
6. M. Ashrafinia, A. Hadadi, D. Sardari *et al.*, *Iran. J. Med. Phys.* **17** (2020) 7.

7. L. Brualla, M. Rodriguez, J. Sempau *et al.*, *Radiat. Oncol.* **14** (2019) 1.
8. A. Girardi, C. Fiandra, F. R. Giglioli *et al.*, *Phys. Med. Biol.* **64** (2019) 1.
9. F. Verhaegen and J. Seuntjens, *Phys. Med. Biol.* **48** (2003) R107.
10. J. Chung, J. Kim, K. Eom *et al.*, *J. Appl. Clin. Med. Phys.* **16** (2015) 302.
11. P. Tsiamas, E. Sajo, F. Cifter *et al.*, *Physica Med.* **30** (2014) 47.
12. Y. Wang, M. K. Khan, J. Y. Ting *et al.*, *Int. J. Radiat. Oncol. Biol. Phys.* **83** (2012) e281.
13. J. Jank, G. Kragl and D. Georg, *Z. Med. Phys.* **24** (2014) 38.
14. S. Ashokkumar, A. Nambiraj, S. N. Sinha *et al.*, *Rep. Pract. Oncol. Radiother.* **20** (2015) 170.
15. S. F. Kry, U. Titt, F. Pönisch *et al.*, *Int. J. Radiat. Oncol. Biol. Phys.* **68** (2007) 1260.
16. M. A. Najem, N. M. Spyrou, Z. Podolyak *et al.*, *Radiat. Phys. Chem.* **95** (2014) 205.
17. A. Mesbahi, *Appl. Radiat. Isot.* **65** (2007) 1029.
18. A. Pichandi, K. M. Ganesh, A. Jerin *et al.*, *Rep. Pract. Oncol. Radiother.* **19** (2014) 322.
19. E. I. Parsai, D. Shvydka, D. Pearson *et al.*, *Appl. Radiat. Isot.* **66** (2008) 1438.
20. S. Yani, I. G. E. Dirgayussa, M. F. Rhani *et al.*, *Smart Sci.* **4** (2016) 87.
21. M. Allahverdi, M. Zabihzadeh, M. Ay *et al.*, *Iran J. Radiat. Res.* **9** (2011) 15.
22. D. W. O. Rogers, B. Walters and I. Kawrakow, *NRCC Report PIRS 0509(A)revL*, in: BEAMnrc Users Manual, National Research Council of Canada, Ottawa (2021)1.
23. C. Ma and D. W. O. Rogers, *NRCC Report PIRS-0509(C)revA*, in: BEAMDP Users Manual National Research Council of Canada, Ottawa (2021) 1.
24. M. Mohammed, E. Chakir, H. Boukhal *et al.*, *J. King Saud Univ. Sci.* **29** (2017) 371.